



ORIGINAL ARTICLE

Efficient removal of organic pollutant by activation of persulfate with magnetic $\text{Co}_3\text{O}_4/\text{CoFe}_2\text{O}_4$ composite

Huixuan Zhang^a, Li-chao Nengzi^b, Yu Liu^a, Yingjie Gao^a, Xiuwen Cheng^{a,b,*}

^a Key Laboratory of Western China's Environmental Systems (Ministry of Education) and Key Laboratory for Environmental Pollution Prediction and Control, Gansu Province, College of Earth and Environmental Sciences, Lanzhou University, Lanzhou 730000, China

^b Academy of Economics and Environmental Sciences, Xichang University, Xichang 615000, China

Received 13 August 2019; accepted 15 March 2020

Available online 4 April 2020

KEYWORDS

$\text{Co}_3\text{O}_4/\text{CoFe}_2\text{O}_4$ composite;
Persulfate;
Rhodamine B;
Sulfate radicals;
Hydroxyl radicals

Abstract In this study, magnetic spinel $\text{Co}_3\text{O}_4/\text{CoFe}_2\text{O}_4$ composite were synthesized by the mechanical mixing of both powdered pristine samples. Then the catalyst was characterized by TEM, SEM, XRD, BET, XPS and VSM measurement. Next, $\text{Co}_3\text{O}_4/\text{CoFe}_2\text{O}_4$ composite was applied to degrade rhodamine B (RhB) in water by activating persulfate. Results showed that $\text{Co}_3\text{O}_4/\text{CoFe}_2\text{O}_4$ composite exhibited high efficiency for removal of RhB, and 95.59% of it could be degraded in 45 min. Besides, the effects of parameters, such as initial pH, PS dosage, $\text{Co}_3\text{O}_4/\text{CoFe}_2\text{O}_4$ composite dosage, initial concentration of RhB and temperature were studied. Also, the effects of coexisting anions on RhB degradation were observed and explained. Furthermore, we conducted the quenching experiment and found that sulfate radical and hydroxyl radicals were the main active radicals in the degradation process. Finally, recycle experiments proved that $\text{Co}_3\text{O}_4/\text{CoFe}_2\text{O}_4$ had a good stability for RhB degradation. In short, $\text{Co}_3\text{O}_4/\text{CoFe}_2\text{O}_4$ composite is a promising catalyst for wastewater treatment.

© 2020 The Author(s). Published by Elsevier B.V. on behalf of King Saud University. This is an open access article under the CC BY-NC-ND license (<http://creativecommons.org/licenses/by-nc-nd/4.0/>).

1. Introduction

Today, water environment pollution is one of the major environmental problems in the world. Among various types of polluted water, printing and dyeing wastewater, as one of the hard-degradable wastewater, is gradually receiving more and more attention (Hou et al., 2016; He et al., 2018). Due to the processing of chemical fiber and other spinning products, the printing and dyeing wastewater contains a large amount of dyes, oils, starch alkalis, resins and inorganic salts, etc. It is

* Corresponding author at: College of Earth and Environmental Sciences, Lanzhou University, Lanzhou 730000, PR China.

E-mail address: chengxw@lzu.edu.cn (X. Cheng).

Peer review under responsibility of King Saud University.



Production and hosting by Elsevier

very difficult to deal with. Most of the dyes are easily dissolved in water in form of cationic (rhodamine B, malachite green, methylene blue, and methyl violet) and anionic (Congo red, methyl orange, and rose Bengal) (Nafey et al., 2017).

Advanced oxidation technology is a new technology which can efficiently remove difficult-to-degrade pollutants from water. In this method, highly active radicals (HO^\cdot , $\text{SO}_4^{\cdot-}$, etc.) can be generated through various routes to degrade pollutants, including Fenton method (Wang et al., 2009), photocatalytic oxidation method (Cheng et al., 2015), electrochemical oxidation method (Li et al., 2013), etc. Among these approaches, $\text{SO}_4^{\cdot-}$ -based technology has received increasing attention due to its higher redox potential (2.5–3.1 V) based on the activation methods compared with HO^\cdot (Lutze et al., 2015; Ghauch and Tuqan, 2012). Apart from these, $\text{SO}_4^{\cdot-}$ has higher selectivity and longer half-life over HO^\cdot in some cases (Ahmed et al., 2012). It can be generated by persulfate (PS) and peroxymonosulfate (PMS) activation through heat (Antonioni et al., 2010; Huang et al., 2002), ultraviolet (Chu et al., 2016; Sharma et al., 2016; Sharma et al., 2015), ultrasound (Gayathri et al., 2010; Chakma et al. 2017; Babu et al. 2017; Neppolian et al., 2010), electron beam (Criquet and Leitner, 2011; Furman et al., 2010); electrochemical (Ahmadi and Ghanbari, 2016; Ghanbari and Martinez-Huitle, 2019; Popat et al., 2019); zero valent metal (Khatri et al., 2018; Devi et al., 2016) and transition metal ions (Xie et al., 2016; Rastogi et al., 2009; Ayoub and Ghauch, 2014; Senthilnathan and Nachiappana, 2015; Sarath et al., 2014; Nidheesh and Rajan, 2016; Asha et al., 2017). Particularly, potassium persulfate ($\text{K}_2\text{S}_2\text{O}_8$), as one of the common source of $\text{SO}_4^{\cdot-}$, attracted much attention due to its moderate cost, high stability, high solubility in aqueous solution, and it exists in the form of solid at room temperature (Zacharias et al., 2016; Lin et al., 2011). In view of economy and operation, choosing transition metal to activate PS is a good choice because it doesn't require energy. Furthermore, the Co^{2+} was proven to be most effective transition metal ions (Anipsitakis and Dionysiou, 2003). However, Co^{2+} is highly soluble in water environments, which could induce health problems (Huang and Huang, 2009; Yang et al., 2009; Ji et al., 2016). In order to overcome this shortcoming, heterogeneous Co catalysts such as CoO , CoO_2 , Co_2O_3 , and Co_3O_4 , have been used to activate PS. Among them, Co_3O_4 , as one of the P-type metal oxide semiconductors, attracted wide attention due to its magnetic (Wang et al., 2015). Besides, owing to its low valence band maximum (VBM), Co_3O_4 has a superior oxidation capacity (Bautista et al., 2008). What's more, spinel ferrites (MFe_2O_4 ($\text{M} = \text{Fe}, \text{Cu}, \text{Co}, \text{Ni}, \text{etc.}$)) have high catalytic activity, stable crystalline structure, extremely low solubility and good magnetic in terms of activating PS in water environment. So they have been taken as very promising candidates (Yang et al., 2009; Zhang et al., 2013; Deng et al., 2013). In particular, spinel cobalt ferrite (CoFe_2O_4) has been confirmed to be one of the efficient catalyst which can activate PMS to degrade organic compounds due to its excellent magnetic property and surface active Co^{2+} (Ren et al., 2015; Liu et al., 2015). Sun et al. (2016) fabricated an octahedral $\text{CoFe}/\text{CoFe}_2\text{O}_4$ submicron composite by a flexible one-pot hydrothermal, which can efficiently activate PMS to decompose methyl orange. Li et al. (2017) successfully

prepared polypyrrole/CNTs- CoFe_2O_4 magnetic nanohybrid (CNTs- CoFe_2O_4 @PPy), which was used as a superior adsorbent and catalyst to remove anionic and cationic dyes according activating PMS. However, at present, there is less research on activating PS with CoFe_2O_4 to produce sulfate radicals for degradation of pollutants. If combine Co_3O_4 with CoFe_2O_4 , the cobalt leaching will reduce and magnetic will strengthen, thus catalysts can be better recycled.

In this study, we first prepared Co_3O_4 by calcination, then synthesized CoFe_2O_4 by a simple one-step hydrothermal method. Subsequently, we combined the two of catalysts by mechanical stirring. Next, the physicochemical properties of $\text{Co}_3\text{O}_4/\text{CoFe}_2\text{O}_4$ composite were analyzed. After this, we evaluated the catalytic activity of $\text{Co}_3\text{O}_4/\text{CoFe}_2\text{O}_4$ by degradation of RhB via the formation of sulfate radicals and hydroxyl radicals by activating PS. Finally, we proposed the possible reaction mechanism towards the degradation of RhB.

2. Materials and methods

2.1. Materials

Ferric nitrate ($\text{Fe}(\text{NO}_3)_3 \cdot 6\text{H}_2\text{O}$), cobalt nitrate ($\text{Co}(\text{NO}_3)_2 \cdot 6\text{H}_2\text{O}$), and potassium persulfate ($\text{K}_2\text{S}_2\text{O}_8$) were purchased from Tianjin Kemiou Chemical Reagent Co. LTD. Cobalt chloride ($\text{CoCl}_2 \cdot 6\text{H}_2\text{O}$), urea ($\text{CO}(\text{NH}_2)_2$) and ascorbic acid ($\text{C}_6\text{H}_8\text{O}_6$) were provided by Sinopharm Chemical Reagent Co. Ltd. Ultra-pure water was used throughout the whole experiment.

2.2. Synthesis of Co_3O_4 powder

In a typical experiment, 5 g of $\text{Co}(\text{NO}_3)_2 \cdot 6\text{H}_2\text{O}$ was placed in a closed ceramic crucible and heated in a muffle furnace at around 400 °C for 4 h. After the furnace cooling to room temperature, Co_3O_4 powder was obtained. All chemicals were of analytical reagent grade and used without any further purification. Ultra-pure water was used throughout this experiment.

2.3. Synthesis of $\text{Co}_2\text{Fe}_2\text{O}_4$ powder

CoFe_2O_4 were synthesized by a simple one-step hydrothermal method. 3.9975 mmol $\text{Fe}(\text{NO}_3)_3 \cdot 9\text{H}_2\text{O}$, 1.995 mmol $\text{CoCl}_2 \cdot 6\text{H}_2\text{O}$, 4.26 mmol $\text{C}_6\text{H}_8\text{O}_6$ and 15 mmol $\text{CO}(\text{NH}_2)_2$ were slowly added to the 100 mL breaker which contained 60 mL distilled water. Afterwards, it was stirred under magnetic for 30 min until dissolved. Subsequently, the mixture was transferred into an autoclave and treated at 160 °C for 6 h. After centrifuging and washing with water and ethanol for several times, the black precipitate was dried at 80 °C for 3 h. Finally, it was calcined in static air at 500 °C for 4 h.

2.4. Synthesis of $\text{Co}_3\text{O}_4/\text{Co}_2\text{Fe}_2\text{O}_4$ composite

The $\text{Co}_3\text{O}_4/\text{CoFe}_2\text{O}_4$ composite was fabricated by the mechanical mixing method. In detail, a certain amount of Co_3O_4 and CoFe_2O_4 powders were dispersed in absolute ethanol and stirred for 2 h under magnetic. After, the powders were dried at 70 °C for 4 h.

2.5. Characterization

In this paper, the surface morphology of $\text{Co}_3\text{O}_4/\text{CoFe}_2\text{O}_4$ composite catalyst was observed by scanning electron microscopy (SEM) at 20 kV. Transmission electron microscopy (TEM) was conducted on a FEI Tecnai F20 transmission electron microscope at an acceleration voltage of 200 kV. The crystal structure, composition and lattice constant of catalysts were measured on a Rigaku D/MAX III-3B X-ray diffractometer (XRD) with $\text{Cu } K\alpha$ ($\lambda = 0.15418 \text{ nm}$) radiation. And the accelerating voltage and applied current were held at 40 kV and 200 mA, respectively. The specific surface area and pore size distribution of samples were measured on an AUTOSORB-1 (Quantachrome Instruments) at 77 K. X-ray photoelectron spectroscopy (XPS) analysis of the catalysts obtained were conducted on PHI-5700 ESCA apparatus with an Al $K\alpha$ X-ray source to explore the elements of the surface, and the binding energies were referenced to adventitious carbon for 284.62 eV. LAKESHORE Model 7304 instrument was used to measure the magnetic properties of catalysts. Magnetic measurement was performed at room temperature by using a physical property measurement system (PPMS, 730 T, LAKE-SHORE, USA)

2.6. Pollutants degradation experiment

As for the organic pollutant degradation tests, RhB was selected to be a typical model contaminant. In each run, a certain amount of catalysts above was added into 50 mL of RhB solution ($10 \text{ mg}\cdot\text{L}^{-1}$) under stirring. The initial pH value of RhB solution was about 5.49 without adjustment. Before to reaction, the suspension was kept in dark for 20 min to ensure the establishment of adsorption/desorption equilibrium between catalysts and rhodamine B. Next, a fixed amount of PS was added to initiate the catalytic reaction. At given time intervals, the collected samples after centrifugation and filtration (through a $0.22 \mu\text{m}$ membrane) were measured at the characteristic peak of 550 nm by using a T6 ultraviolet-visible spectrophotometer.

3. Results and discussion

3.1. SEM and TEM analysis

The morphological observations clearly indicated the successful synthesis of $\text{Co}_3\text{O}_4/\text{CoFe}_2\text{O}_4$ composite. As shown in Fig. 1a, a large amount of nanoparticles gathered together. However, it was difficult to distinguish Co_3O_4 and CoFe_2O_4 since both of them were spherical particles. From the TEM image (Fig. 1b), a very serious aggregation phenomenon was also exhibited. Besides, EDXA elemental mapping and the selected energy dispersive spectrum (EDS) were also analyzed in order to see the element dispersion of the $\text{Co}_3\text{O}_4/\text{CoFe}_2\text{O}_4$ composite. As displayed in Fig. 1c-f, the composite was composed of Co, Fe and O elements.

3.2. XRD analysis

XRD patterns further indicated the crystal structure of the catalysts. Seen from Fig. 2, The diffraction peaks of pure Co_3O_4

appearing at 18.9° , 31.2° , 36.8° , 45.2° , 59.6° and 65.2° could be perfectly assigned to the (1 1 1), (2 2 0), (3 1 1), (4 0 0), (5 1 1) and (4 4 0) crystal planes of Co_3O_4 respectively. For single CoFe_2O_4 , the peaks at 30.2° , 35.5° , 42.3° , 57.2° , and 62.9° were detected, which could be indexed to the cubic spinel structure of cobalt ferrite (Li et al., 2011). As for pure $\text{Co}_3\text{O}_4/\text{CoFe}_2\text{O}_4$ catalyst, all the characteristic peaks belonging to Co_3O_4 didn't shift. However, due to the lower doping content of CoFe_2O_4 nanoparticles, only the peak at 35.5° could be observed, which could be attributed to the (3 1 1) crystal plane of cobalt ferrite, the other diffraction peaks of CoFe_2O_4 were not be directly detected.

3.3. Nitrogen adsorption-desorption

It is well known that the catalytic properties of materials are also closely related to their specific surface area and porosity. We studied the structural properties of pure Co_3O_4 and $\text{Co}_3\text{O}_4/\text{CoFe}_2\text{O}_4$ composites by nitrogen adsorption analysis. As shown in Fig. 3, according to the IUPAC classification, the isotherms of pure Co_3O_4 and $\text{Co}_3\text{O}_4/\text{CoFe}_2\text{O}_4$ were type IV, characteristic for mesoporous structures, with relatively similar H_2 hysteresis loops. The specific surface area of $\text{Co}_3\text{O}_4/\text{CoFe}_2\text{O}_4$ was calculated to be $13.894 \text{ m}^2\cdot\text{g}^{-1}$, which was larger than that of pure Co_3O_4 ($12.143 \text{ m}^2\cdot\text{g}^{-1}$). For pure Co_3O_4 , the BJH pore size analysis on the desorption branch exhibited only a peak centered at 35.04 nm. The pore size distribution of $\text{Co}_3\text{O}_4/\text{CoFe}_2\text{O}_4$ composite also with one peak at 36.09 nm. Both of the samples had the good homogeneity of the pores. Similarly, the $\text{Co}_3\text{O}_4/\text{CoFe}_2\text{O}_4$ composite had a bigger pore volume ($0.146 \text{ m}^3\cdot\text{g}^{-1}$) compared with pure Co_3O_4 ($0.132 \text{ m}^3\cdot\text{g}^{-1}$). Large accessible surface area and numerous pores made the catalyst to provide more reactive sites, thus enhanced the catalytic performance.

3.4. XPS measurement

The XPS spectra of the $\text{Co}_3\text{O}_4/\text{CoFe}_2\text{O}_4$ composite were recorded and given in Fig. 4. As shown in Fig. 4a, the de-convolution of the Co 2p peak in CoFe_2O_4 exhibited four peaks. From CoFe_2O_4 , the peak at 780.7 eV was attributed to Co $2p_{3/2}$, while the peak at 795.65 eV was caused by Co $2p_{1/2}$. What's more, the peaks of the satellites at about 785.75 eV and 802.67 eV were two shake-up type peaks of Co at the high binding energy side of the Co $2p_{3/2}$ and Co $2p_{1/2}$ edges. However, when Co_3O_4 was combined with CoFe_2O_4 , the de-convolution of the Co 2p peak in $\text{Co}_3\text{O}_4/\text{CoFe}_2\text{O}_4$ composite exhibited six peaks. The peaks at 779.59 eV and 794.36 eV were assigned to Co^{3+} , whereas the peaks at 781.07 eV and 795.97 eV were attributed to Co^{2+} (Li et al., 2011). Besides, the peaks at 788.97 eV and 803.99 eV belonged to the shake-up satellite peaks (Deng et al., 2016). This suggested that the Co species existed in the form of Co^{2+} and Co^{3+} in the $\text{Co}_3\text{O}_4/\text{CoFe}_2\text{O}_4$ composite. In addition, from the peak area, it could be determined that the content of Co^{3+} was much more than that of Co^{2+} , which also indicated that the content of Co_3O_4 was much higher than that of CoFe_2O_4 , which was consistent with the results of SEM and TEM. The Fe 2p XPS spectra of the CoFe_2O_4 and the $\text{Co}_3\text{O}_4/\text{CoFe}_2\text{O}_4$ samples were presented in Fig. 4b. Two peaks at a binding energy of 710.75 eV and 724 eV, corresponding to

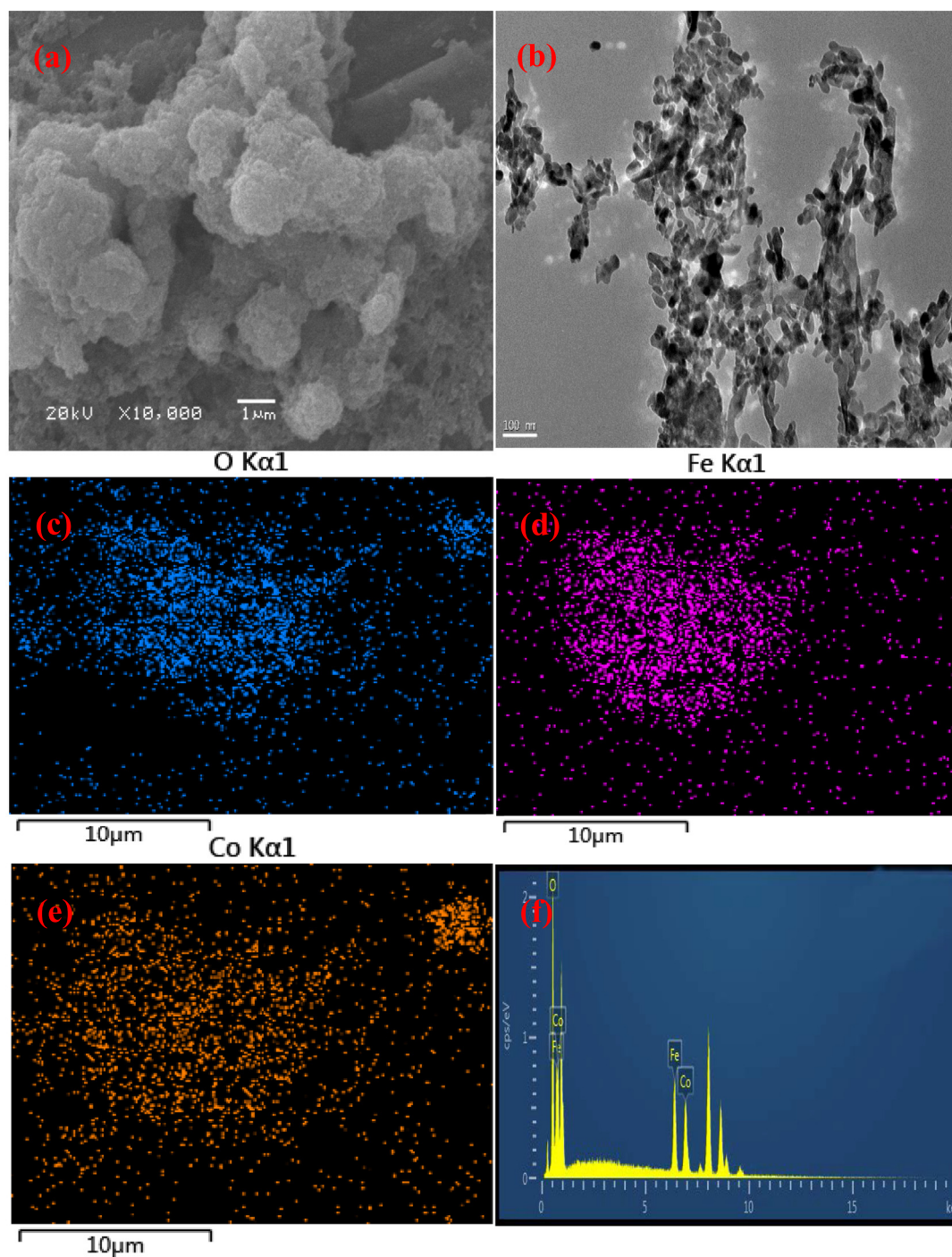


Fig. 1 TEM image (a), SEM image (b), EDXA elemental mapping (Co, Fe and O elements (c–e)) and EDS spectroscopy (f) of $\text{Co}_3\text{O}_4/\text{CoFe}_2\text{O}_4$ composite.

$\text{Fe } 2p_{3/2}$ and $\text{Fe } 2p_{1/2}$, respectively, which suggested the presence of Fe^{3+} . Furthermore, the peak at 717.35 eV and 732.66 eV were assigned to shake-up satellite peaks (Salunkhe et al., 2015). However, it could be observed that the binding energy of $\text{Fe } 2p_{1/2}$ shifted from 724 eV of the CoFe_2O_4 to 722.35 eV of the $\text{Co}_3\text{O}_4/\text{CoFe}_2\text{O}_4$ composite. Seen from Fig. 4c, the high resolution XPS spectrum of O1s (CoFe_2O_4)

included two peaks with binding energy at 529.59 and 531.31 eV, corresponding to the surface lattice oxygen species (O_{latt}) and the surface adsorbed oxygen species (O_{ads}), respectively. But it had a slightly decrease in $\text{Co}_3\text{O}_4/\text{CoFe}_2\text{O}_4$. Compared with pure CoFe_2O_4 , the varied binding energy values of Co 2p, Fe 2p and O 1s for the $\text{Co}_3\text{O}_4/\text{CoFe}_2\text{O}_4$ composite meant the rapid transfer of electrons.

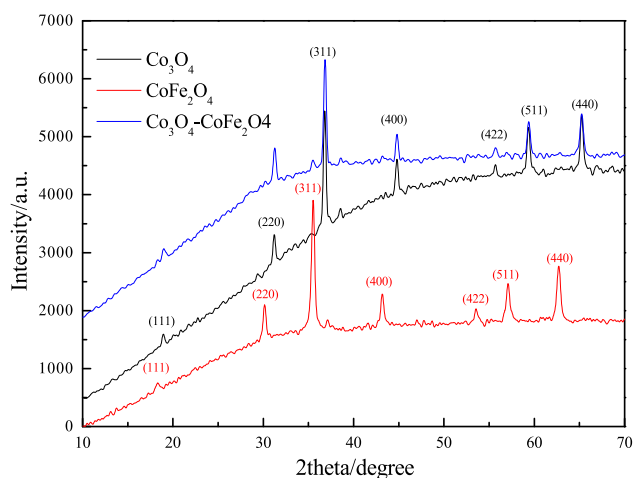


Fig. 2 XRD patterns of Co_3O_4 , CoFe_2O_4 and $\text{Co}_3\text{O}_4/\text{CoFe}_2\text{O}_4$ samples.

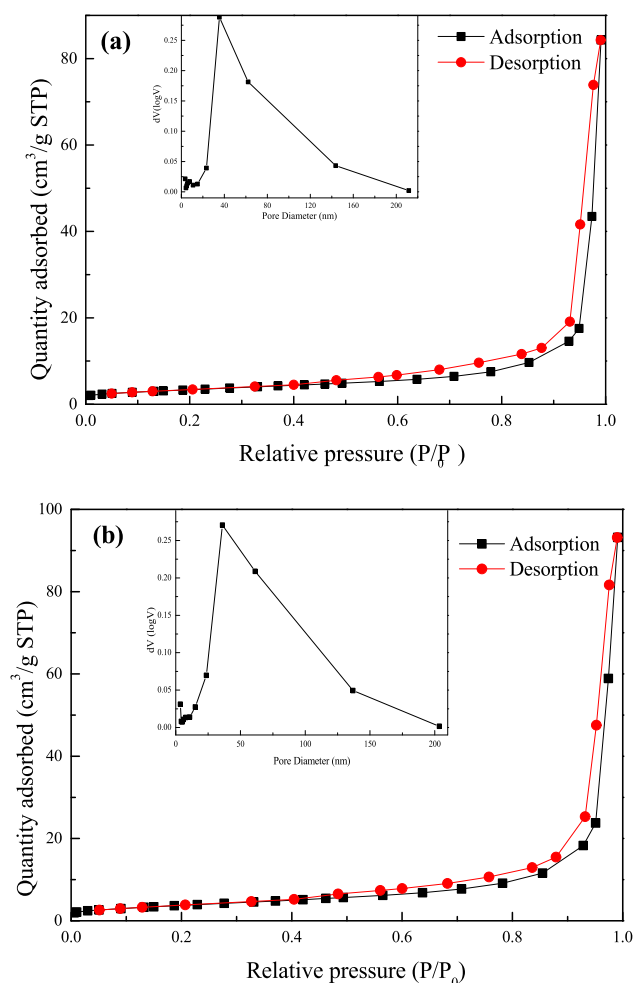


Fig. 3 N_2 adsorption and desorption isotherm and BJH pore-size distribution of Co_3O_4 (a) and $\text{Co}_3\text{O}_4/\text{CoFe}_2\text{O}_4$ (b).

3.5. VSM analysis

As is known to all, pulverous catalysts were difficult to separate and recycle from the slurry system, which caused

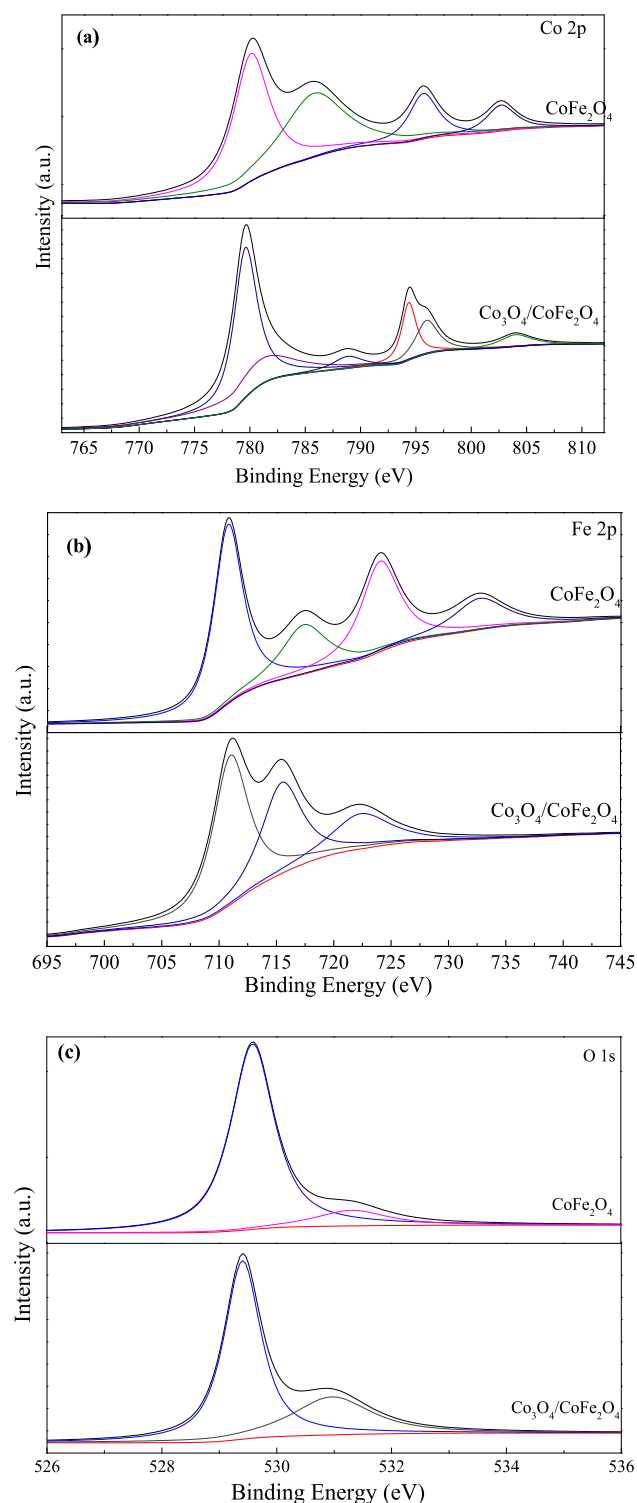


Fig. 4 High-resolution XPS spectrum of Co 2p (a), Fe 2p (b) and O 1s (c) for CoFe_2O_4 and $\text{Co}_3\text{O}_4/\text{CoFe}_2\text{O}_4$ samples.

the practical bottleneck of applications. In this paper the magnetic property of the $\text{Co}_3\text{O}_4/\text{CoFe}_2\text{O}_4$ composite was confirmed by the M–H analysis. As given in Fig. 5, the saturation magnetization (M_S) value of $\text{Co}_3\text{O}_4/\text{CoFe}_2\text{O}_4$ composite was $6.13 \text{ emu}\cdot\text{g}^{-1}$, which was lower than that of pure $\text{Co}_3\text{O}_4/\text{CoFe}_2\text{O}_4$ sample ($59.62 \text{ emu}\cdot\text{g}^{-1}$). This decrease could

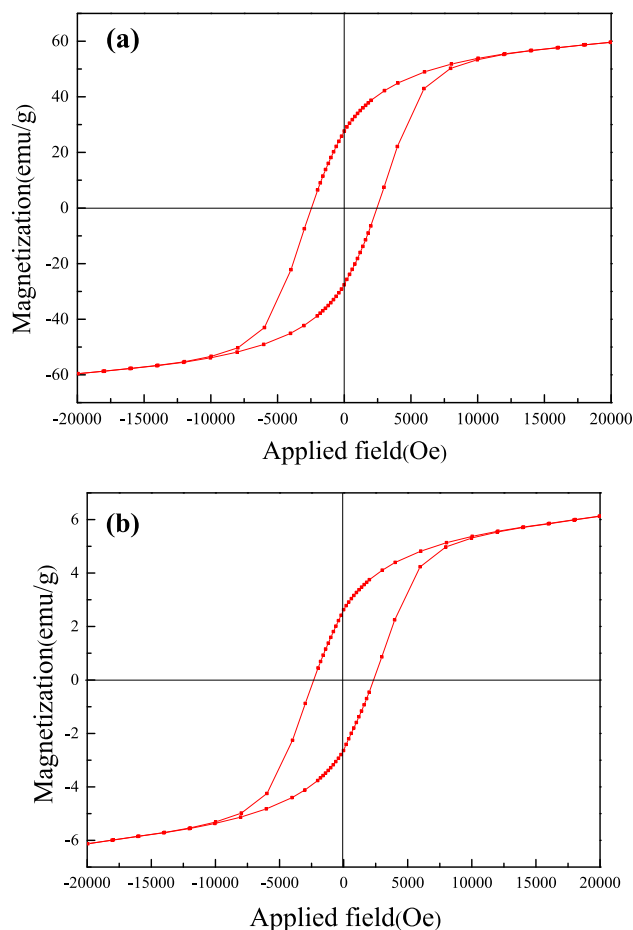


Fig. 5 Hysteresis loop diagram of CoFe_2O_4 (a) and $\text{Co}_3\text{O}_4/\text{CoFe}_2\text{O}_4$ (b) sample.

be explained that the introduced Co_3O_4 sample was non-magnetic. Despite this, $\text{Co}_3\text{O}_4/\text{CoFe}_2\text{O}_4$ composite still performed good magnetic property.

3.6. Degradation performance

3.6.1. Activation of PS by $\text{Co}_3\text{O}_4/\text{CoFe}_2\text{O}_4$ composite for RhB degradation

Fig. 6 exhibited the degradation of RhB under different conditions. As seen from **Fig. 6**, the catalyst alone did not substantially remove RhB, only 6.61%, 2.09% and 8.08% of RhB was removed by CoFe_2O_4 , Co_3O_4 and $\text{Co}_3\text{O}_4/\text{CoFe}_2\text{O}_4$ composite, respectively. The low removal efficiencies might be due to the weak adsorption capacity of these materials. Besides, 32.15% RhB could be removed by PS in the absence of activator owing to the high oxidation potential of PS (2.01 V). Also, 36.56% of RhB was removed in 45 min in $\text{CoFe}_2\text{O}_4/\text{PS}$ system, suggesting that CoFe_2O_4 alone could hardly efficiently activate PS. However, the degradation efficiency of RhB was greatly enhanced in the presence of both Co_3O_4 spinel and PS. The $\text{Co}_3\text{O}_4/\text{CoFe}_2\text{O}_4$ composite performed best degradation of RhB, which could almost completely remove the RhB (95.59%), which was attributed to the coupling effect of Co_3O_4 and CoFe_2O_4 .

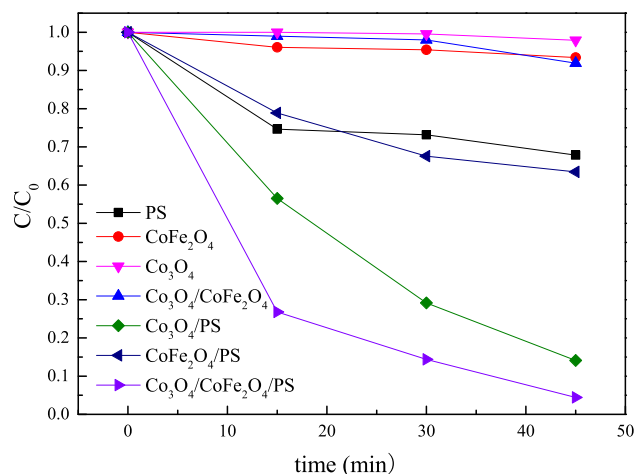


Fig. 6 Removal curves of RhB under different reaction conditions. Experimental conditions: catalyst = $0.5 \text{ g}\cdot\text{L}^{-1}$, PS = $0.5 \text{ g}\cdot\text{L}^{-1}$, pH = 5.49 (natural) and RhB = $10 \text{ mg}\cdot\text{L}^{-1}$.

3.6.2. Effects of persulfate concentration, catalyst dosage, solution pH and reaction temperature

The degradation of RhB in $\text{Co}_3\text{O}_4/\text{CoFe}_2\text{O}_4/\text{PS}$ system with different PS doses was investigated and exhibited in **Fig. 7a**. The removal efficiency of RhB increased from 8.08% to 96.64% with the PS dosage increasing from 0 to $0.9 \text{ g}\cdot\text{L}^{-1}$, respectively. This showed that PS provided a source of $\text{SO}_4^{\cdot-}$ and RhB removal was indeed caused by oxidative degradation, rather than a simple adsorption by the catalyst. However, excessive persulfate would cause self-quenching of $\text{SO}_4^{\cdot-}$ (Liang et al., 2004) (reaction (1) and (2)), the degradation efficiencies of RhB were similar when the amount of PS was $0.5 \text{ g}\cdot\text{L}^{-1}$ and $0.9 \text{ g}\cdot\text{L}^{-1}$. In addition, the reaction stoichiometric efficiency (RSE) was used to evaluate the utilization efficiency of PS according previous studies (Jaafarzadeh et al., 2017; Amasha et al., 2018). The calculated RSE% was the largest when the PS concentration was $0.5 \text{ g}\cdot\text{L}^{-1}$. Thus $0.5 \text{ g}\cdot\text{L}^{-1}$ was selected as the optimal concentration of PS and used in later experiments.

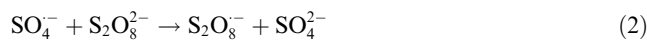


Fig. 7b showed the degradation of RhB under different $\text{Co}_3\text{O}_4/\text{CoFe}_2\text{O}_4$ dosages ($0\text{--}0.9 \text{ g}\cdot\text{L}^{-1}$). Generally speaking, higher the $\text{Co}_3\text{O}_4/\text{CoFe}_2\text{O}_4$ dosage resulted in higher RhB degradation efficiency, which could be attributed to the increased number of active sites. As exhibited in **Fig. 6b**, the degradation efficiency of RhB increased as the amount of catalyst increased to $0.5 \text{ g}\cdot\text{L}^{-1}$, and then hardly increased. Although a large number of catalysts could provide more active sites to activate PS, it would also capture the active radicals (Wang et al., 2018). In addition, high concentrations of catalysts would gather together, thus reduced the available amount of active sites.

Due to the wide range of pH in natural water bodies, it was very important to study the optimal reaction conditions for the removal of refractory organic pollutants using $\text{Co}_3\text{O}_4/\text{CoFe}_2\text{O}_4/\text{PS}$ system. In this study, the effects of initial solution pH on RhB removal were tested in a broad pH

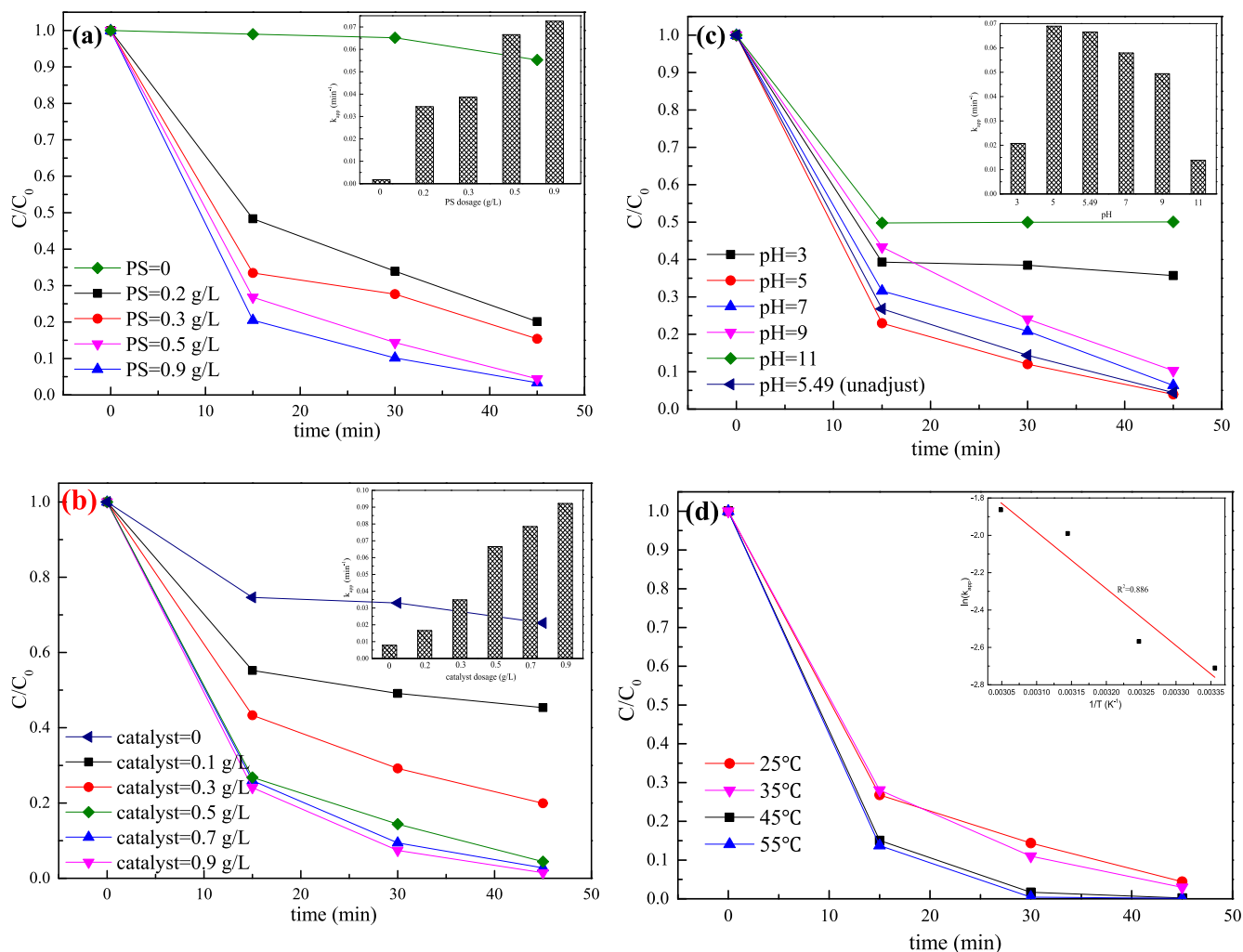


Fig. 7 Influence of initial pH (a) amount of persulfate (b) amount of catalyst (c) initial temperature (d) on RhB degradation. Experimental conditions: catalyst = 0.5 g·L⁻¹, PS = 0.5 g·L⁻¹, pH = 5.49 (natural) and RhB = 10 mg·L⁻¹.

ranging from 3.0 to 11.0 at PS dosage of 0.5 g·L⁻¹ and the Co₃O₄/CoFe₂O₄ dosage of 0.5 g·L⁻¹ (Fig. 7c). Among them, 5.49 was the original pH of the RhB solution formulated. It was noted that both extremely acidic (pH = 3) and alkaline (pH = 11) conditions were unfavorable for the degradation process. Co₃O₄/CoFe₂O₄ composite was easily dissolved to release metal ions under acidic solution, as a result, the activity of the catalyst was greatly reduced (Wang et al., 2011), which only degraded 64.28% of RhB (pH = 3). In addition, hydrogen ion might scavenge SO₄⁻ and ·OH (reaction (3) and (4)) (Ahmadi et al., 2017; Ghanbari et al., 2019). The best degradation of RhB was achieved at pH of 5 in a Co₃O₄/CoFe₂O₄/PS system, then started to fall. The k_{app} values of RhB degradation with initial pH of 3, 5, 5.49, 7, 9 and 11 were 2.07×10^{-2} , 6.89×10^{-2} , 6.65×10^{-2} , 5.80×10^{-2} , 4.94×10^{-2} and 3.82×10^{-3} min⁻¹, respectively. According to the literature, the pH_{pzc} of CoFe₂O₄ and Co₃O₄ was 5.96 and 8.5, respectively (Du et al., 2016; Zhang et al., 2016). When the Co₃O₄/CoFe₂O₄ composite was dispersed in water (pH < 5.96), the surface of the catalyst was positively charged, which would increase the coverage of the hydroxyl group (-OH) from H₂O, which was beneficial to the formation of

active radicals. At higher pH values, the electrostatic repulsion between the S₂O₈²⁻ and the Co₃O₄/CoFe₂O₄ surface might limit the contact of the PS onto the catalyst surface. Besides, SO₄⁻ could be converted into ·OH by hydrolysis. For aromatic compounds, SO₄⁻ reacted with them by means of electron transfer, and SO₄⁻ was more prone to electron transfer reactions than ·OH (Neta et al., 1977; Buxton et al., 1988). So only 49.95% of RhB was removed when pH was 11.



What's more, the effect of temperature on RhB degradation was also evaluated by varying the reaction temperatures, which was exhibited in Fig. 7d. When the temperature was increased from 25 °C to 55 °C, it could be observed that the degradation efficiency of RhB was greatly improved. When the temperature was 55 °C, the degradation efficiency of RhB could reach nearly 100% within 30 min. These results indicated that the degradation of RhB depended on the temperature. A higher temperature could accelerate the decomposition of PS and the movement of oxidant, intermediates, RhB

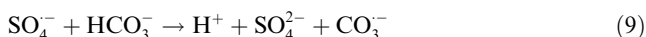
molecules (Chen et al., 2014). According to the Arrhenius equation (5):

$$\ln(k) = \ln A - \frac{E_a}{RT} \quad (5)$$

Among them, A is the Arrhenius constant, E_a is the apparent activation energy ($\text{kJ}\cdot\text{mol}^{-1}$), R is the universal gas constant ($8.314 \times 10^{-3} \text{ kJ}\cdot\text{mol}^{-1}\cdot\text{K}^{-1}$), and T is the absolute temperature (K). In this experiment, the activation energy of the reaction was calculated as $25.32 \text{ kJ}\cdot\text{mol}^{-1}$, which implied the intrinsic chemical reaction of the $\text{Co}_3\text{O}_4/\text{CoFe}_2\text{O}_4/\text{PS}$ system. Furthermore, compared with other similar materials (Deng et al., 2018; Rida et al., 2018), the $\text{Co}_3\text{O}_4/\text{CoFe}_2\text{O}_4$ in this article exhibited the lower activation energy, indicating it could more easily activate PS.

3.6.3. Effect of co-existing ions

In practice, a large amount of salts were usually added in various dyeing processes and might affect the active radical chain reaction in $\text{SO}_4^{\cdot-}$ based AOP (Li et al., 2015). In this paper, the effects of Cl^- , NO_3^- and HCO_3^- that commonly occurred in real dye wastewater on RhB degradation were evaluated. As shown in Fig. 8, different inorganic anions exhibited different inhibiting effects on the RhB degradation. As seen from Fig. 8a, chloride ion inhibited the degradation of RhB, and the degradation efficiency of RhB decreased with increasing chloride ion concentration. Compared to the case where Cl^- was not added, only 88.18% of RhB was degraded in the existence of 40 mM Cl^- . It had been reported that chloride ions could act as sinks for HO^\cdot and $\text{SO}_4^{\cdot-}$ to produce less reactive chlorine species Cl_2 , HOCl^- , Cl^\cdot and $\text{Cl}_2^{\cdot-}$ (reaction (6), 7 and 8), thereby severely inhibiting the degradation process of RhB (Du et al., 2016; Sharma et al., 2015; Feng et al., 2017). What's more, NO_3^- also had an apparently inhibition effect towards the removal of RhB. This was mainly because NO_3^- can react with the catalyst, resulting in a decrease in catalytic efficiency (Li et al., 2013; Gordon et al., 2013). It was worth noting that the most significant decrease was observed after adding HCO_3^- to the reaction system. In fact, HCO_3^- was an inorganic radical scavenger, which could react with HO^\cdot ($k = 8.5 \times 10^6 \text{ M}^{-1}\cdot\text{s}^{-1}$) and $\text{SO}_4^{\cdot-}$ ($k = 1.6 \times 10^6 \text{ M}^{-1}\cdot\text{s}^{-1}$) quickly, thus producing less reactive carbonate radicals (reaction (9), 10, 11 and 12) (Lin and Wu, 2014; Zuo et al., 1999).



3.6.4. Free radical quenching studies

In order to reveal the activation mechanism, we need to identify the main radical species in the $\text{Co}_3\text{O}_4/\text{CoFe}_2\text{O}_4/\text{PS}$ system

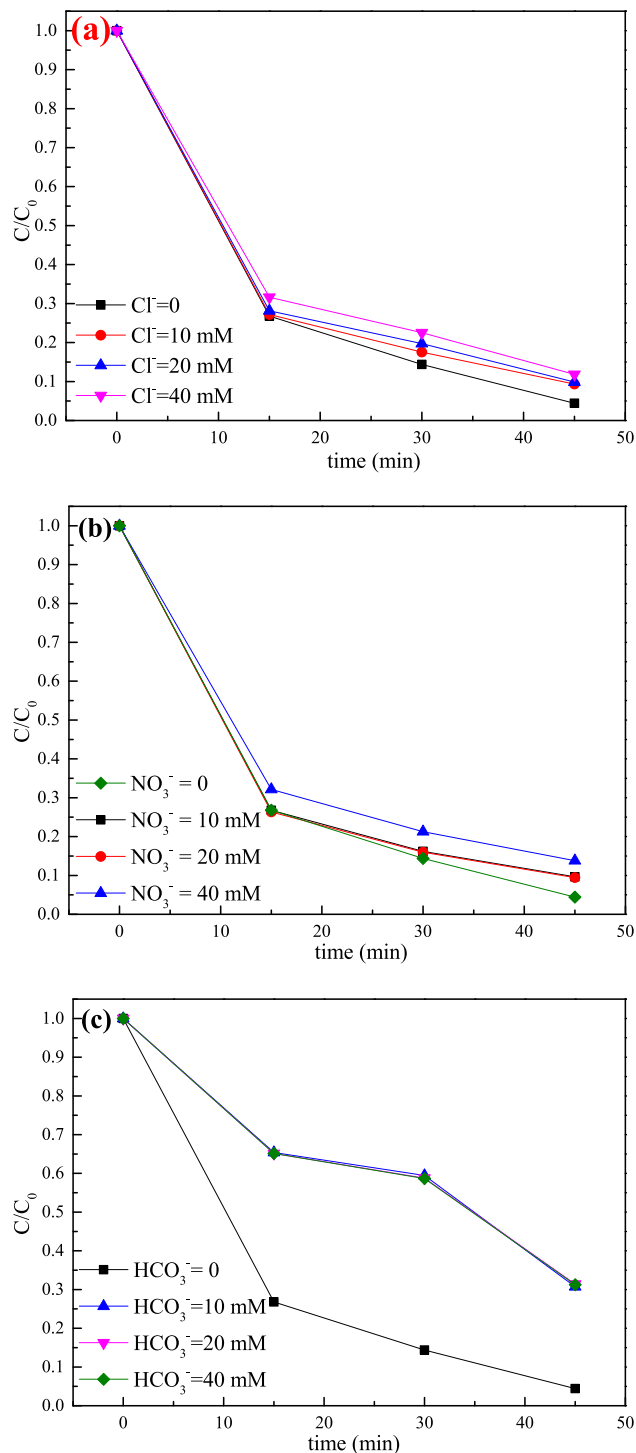


Fig. 8 Effect of (a) Cl^- , (b) NO_3^- and (c) HCO_3^- on the degradation of RhB. Experimental conditions: catalyst = $0.5 \text{ g}\cdot\text{L}^{-1}$, PS = $0.5 \text{ g}\cdot\text{L}^{-1}$, pH = 5.49 (natural) and RhB = $10 \text{ mg}\cdot\text{L}^{-1}$.

for the degradation of RhB. It had been reported that activation of PS mediated by transition metals or metal oxides produced two main types of active radicals, namely $\text{SO}_4^{\cdot-}$ and $\cdot\text{OH}$. As we all know, Methanol (MeOH) is an effective scavenger both for $\cdot\text{OH}$ ($4.6\text{--}9.7 \times 10^8 \text{ M}^{-1}\cdot\text{s}^{-1}$) and $\text{SO}_4^{\cdot-}$ ($1.1\text{--}2.5 \times 10^7 \text{ M}^{-1}\cdot\text{s}^{-1}$). Tert-butanol (t-BuOH) could quickly capture $\cdot\text{OH}$ ($k_{\text{OH}} = (3.8\text{--}7.6) \times 10^8 \text{ M}^{-1}\cdot\text{s}^{-1}$) (Chen et al.,

2005). However, it is reported that isopropanol (IPA) could react with both free and adsorbed hydroxyl radicals (Rivas et al., 2015), which had a more significant inhibiting effect for the degradation of pollutant. In this study, we choose isopropanol and methanol as scavengers to conduct quenching experiments. As seen in Fig. 9, when IPA and MeOH were added, the degradation efficiency of RhB were only 82.46% and 57.23%, respectively. Clearly, the inhibition of MeOH was significantly higher than that of IPA, which indicated that $\text{SO}_4^{\cdot-}$ and $\cdot\text{OH}$ were the main radical in this system, and the contribution of $\text{SO}_4^{\cdot-}$ was larger than $\cdot\text{OH}$.

3.7. Mechanism analysis

Fig. 10a and b presented the XPS of Co 2p and O 1s of the catalysts before and after oxidation process. After PS reacted with $\text{Co}_3\text{O}_4/\text{CoFe}_2\text{O}_4$ composite, the position of the Co 2p peak had a little shift and the area of peaks decreased, indicating that the fraction of $\text{Co}^{2+}/\text{Co}^{3+}$ changed after used. From the deconvolution of Co 2p envelop (Fig. 10a), the proportion of Co^{2+} dropped from 47.96% to 45.27% of Co specie, which implied that the valence state of cobalt increased from Co^{2+} to Co^{3+} due to transferring electrons to PS to generate $\text{SO}_4^{\cdot-}$. Fortunately, the binding energy of the two main peaks was basically unchanged, which indicated that the catalyst was well regenerated. In the case of O 1s spectra (Fig. 10b), the $\text{O}_{\text{ads}}/\text{O}_{\text{latt}}$ ratio had changed and the proportion of O_{ads} had increased from 31.17% to 35.09% and the proportion of O_{latt} reduced from 68.83% to 64.91%, indicating that both of them are involved during the degradation process. The increase of O_{ads} concentration might be ascribed to the formation of Co-OH and Fe-OH groups adsorbed on the $\text{Co}_3\text{O}_4/\text{CoFe}_2\text{O}_4$ surface, which might contribute to the enhancement of the PS activation process.

Based on XPS analysis and other findings, the catalytic mechanism of PS activation by $\text{Co}_3\text{O}_4/\text{CoFe}_2\text{O}_4$ composite was proposed. As shown from Fig. 10c, Co^{2+} and Fe^{3+} were main active centers in $\text{Co}_3\text{O}_4/\text{CoFe}_2\text{O}_4/\text{PS}$ system. Generally speaking, PS could react with Co^{2+} and Fe^{2+} to produce

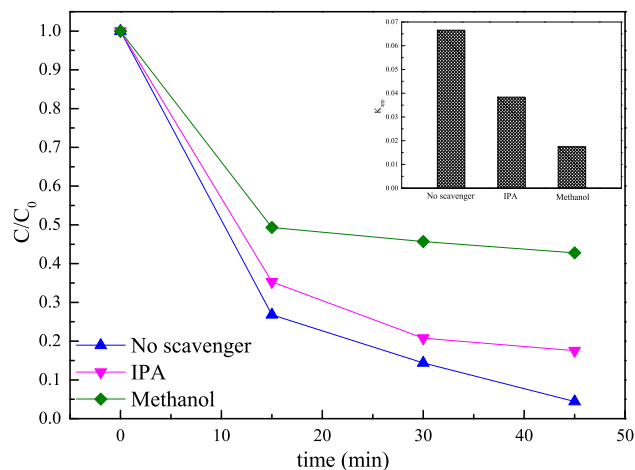
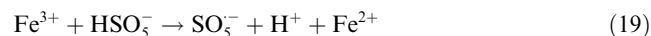
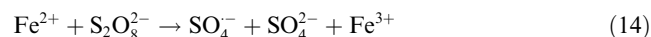
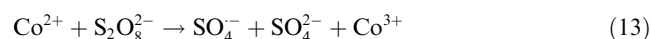


Fig. 9 Effects of different scavengers on PS oxidation for RhB degradation. Experimental conditions: catalyst = $0.5 \text{ g}\cdot\text{L}^{-1}$, PS = $0.5 \text{ g}\cdot\text{L}^{-1}$, pH = 5.49 (natural) and RhB = $10 \text{ mg}\cdot\text{L}^{-1}$ (The inset shows pseudo-first-order rate constants).

$\text{SO}_4^{\cdot-}$, and simultaneously generate Co^{3+} and Fe^{3+} (reaction (13) and (14)). In addition, the conduction band of CoFe_2O_4 was more negative than the Co_3O_4 . When Co_3O_4 combined with CoFe_2O_4 , the heterojunction was rapidly formed and electrons were more easily transferred from CoFe_2O_4 to Co_3O_4 , which promoted the regeneration of Co^{2+} (reaction (15)), which was consistent with the XPS analysis. However, due to the transfer of electron from CoFe_2O_4 to Co_3O_4 , only a few portion of Fe^{3+} could be converted to Fe^{2+} to activate PS (reaction (16)). Fortunately, $\text{S}_2\text{O}_8^{2-}$ could produce HSO_5^- by hydrolysis under acidic condition, therefore Co^{3+} and Fe^{3+} could react with HSO_5^- to achieve the regeneration of Co^{2+} and Fe^{2+} (reactions (17), (18) and (19)). In addition, $\text{SO}_4^{\cdot-}$ could also react with H_2O to produce $\text{HO}\cdot$ (reaction (20)). Ultimately, all these radicals generated further degraded RhB.



3.8. Stability of the catalyst

The repeatability and stability of catalysts are key factors in actual application of persulfate activation. In this study, the recycling experiment was conducted by the sample recovery method of centrifugation and drying. Fig. 11a exhibited the RhB removal in successive four cycles with recycled $\text{Co}_3\text{O}_4/\text{CoFe}_2\text{O}_4$ composite. It was clearly that the $\text{Co}_3\text{O}_4/\text{CoFe}_2\text{O}_4$ composite maintained its performance among the four cycles. $\text{Co}_3\text{O}_4/\text{CoFe}_2\text{O}_4$ composite catalyst could still degrade 85.49% RhB after 4 cycles. In addition, we tested the XRD pattern of the fresh and used $\text{Co}_3\text{O}_4/\text{CoFe}_2\text{O}_4$ composite, which were exhibited in Fig. 11b. Obviously, the used $\text{Co}_3\text{O}_4/\text{CoFe}_2\text{O}_4$ composite maintained the stable crystal structure without phase transition. These indicated that the $\text{Co}_3\text{O}_4/\text{CoFe}_2\text{O}_4$ composite catalyst as-prepared had a good practical potential, which could provide the possibility of practical application in future.

4. Conclusion

In the present study, a novel magnetic catalyst was synthesized, which was applied for PMS activation to achieve effective RhB degradation. It was found that the degradation of RhB was highly pH-dependent with a higher degradation efficiency near the weakly acidic pH. The maximum degradation efficiency was obtained at pH of 5, where 96.05% of RhB was removed (the persulfate concentration of $0.5 \text{ g}\cdot\text{L}^{-1}$, catalyst dosage of $0.5 \text{ g}\cdot\text{L}^{-1}$ and reaction temperature of 25°C).

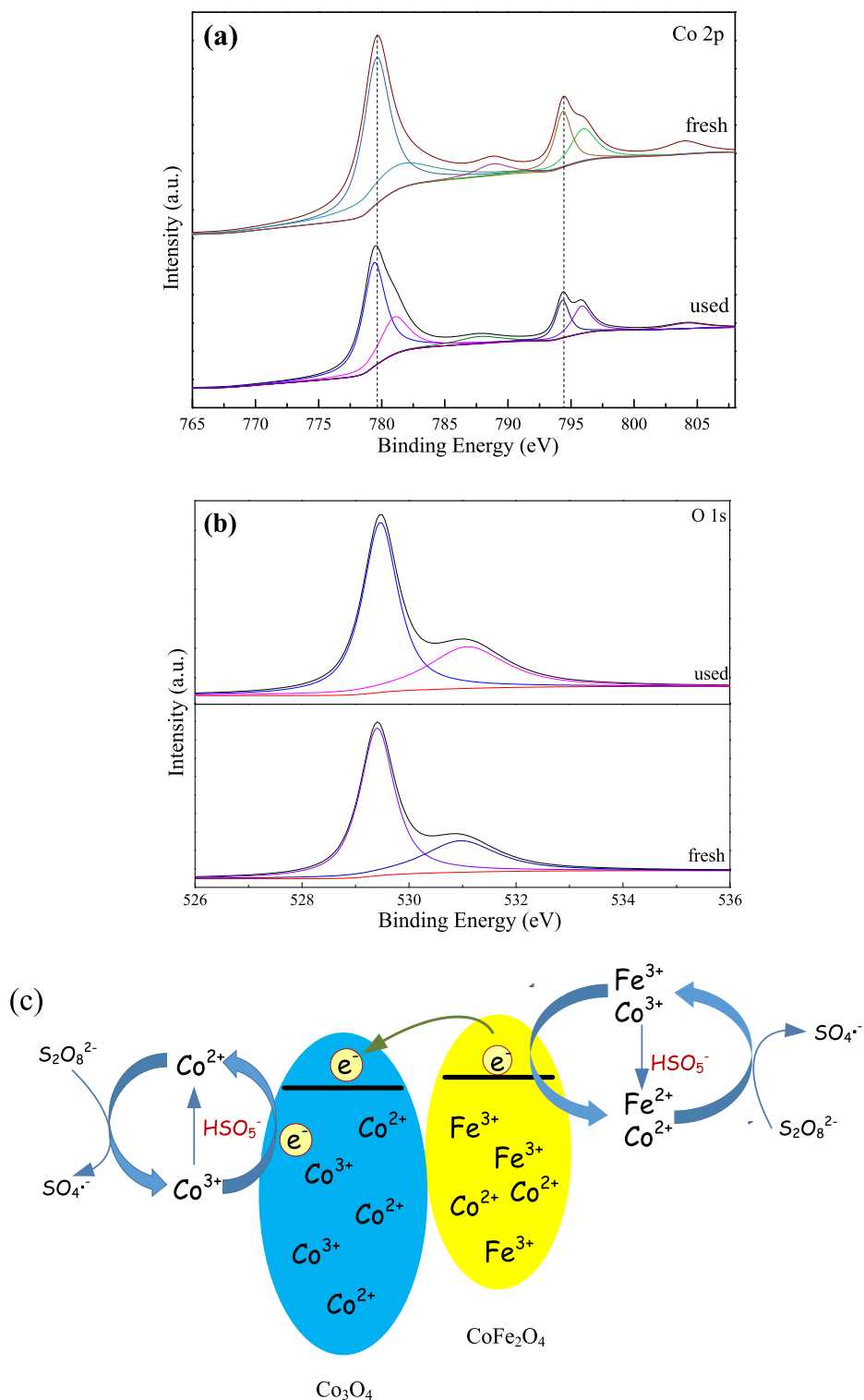


Fig. 10 (a) Co 2p and (b) O 1s XPS envelop of the fresh and used $\text{Co}_3\text{O}_4/\text{CoFe}_2\text{O}_4$ catalyst; (c) Mechanism for RhB degradation by $\text{Co}_3\text{O}_4/\text{CoFe}_2\text{O}_4/\text{PS}$ system.

What's more, naturally occurring species (Cl^- , NO_3^- and HCO_3^-) exhibited inhibitory effects on RhB degradation, especially at higher concentrations. Quenching experiment showed that sulfate radicals were the main active species. Furthermore, $\text{Co}_3\text{O}_4/\text{CoFe}_2\text{O}_4$ composite performed good magnetic

property, which could be easily separated through external magnetic and recycled from the aqueous solution. In addition, recycle experiments was conducted, in which the degradation efficiency of RhB could still reach 85.49% after 4 cycles. Finally, the enhanced mechanism was proposed. Overall, this

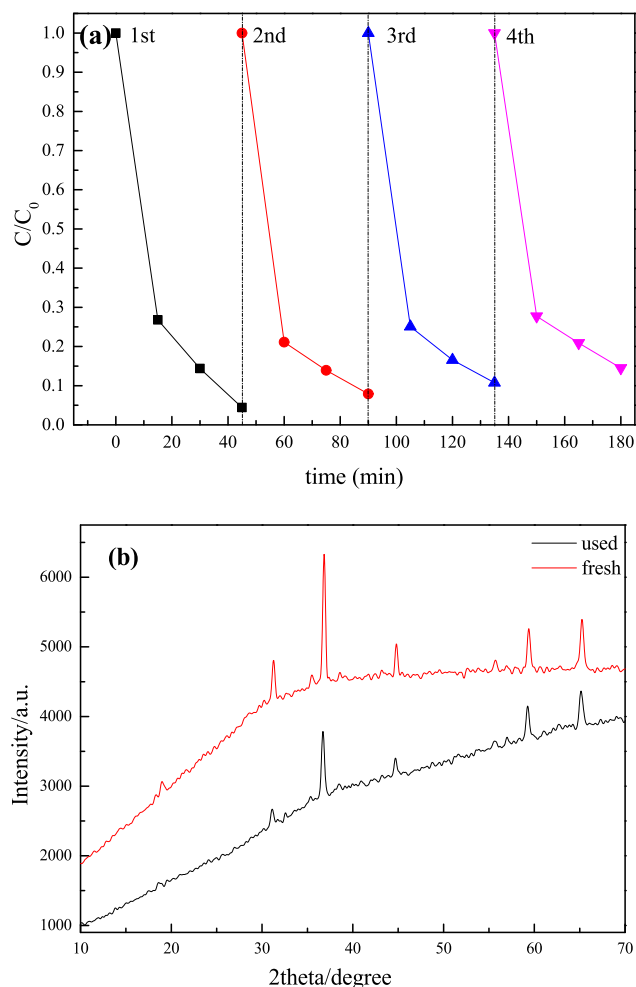


Fig. 11 (a) Reusability of $\text{Co}_3\text{O}_4/\text{CoFe}_2\text{O}_4$ composite for RhB degradation. Experimental conditions: catalyst = $0.5 \text{ g}\cdot\text{L}^{-1}$, PS = $0.5 \text{ g}\cdot\text{L}^{-1}$, pH = 5.49 (natural) and RhB = $10 \text{ mg}\cdot\text{L}^{-1}$; (b) XRD patterns of fresh and used $\text{Co}_3\text{O}_4/\text{CoFe}_2\text{O}_4$.

paper provided a viable strategy for the fabrication of high-efficient recyclable catalysts which could be used in the treatment of printing and dyeing wastewater.

Acknowledgment

This work was kindly funded by National Natural Science Foundation of China (51978319), Fundamental Research Funds for the Central Universities (lzujbky-2017-it98), National College student innovation and Entrepreneurship training program of Lanzhou University and Key Laboratory of Comprehensive and Highly Efficient Utilization of Salt Lake Resources, Qinghai Institute of Salt Lake, Chinese Academy of Sciences.

References

Ahmadi, M., Ghanbari, F., 2016. Optimizing COD removal from greywater by photoelectro-persulfate process using Box-Behnken design: assessment of effluent quality and electrical energy consumption. *Environ. Sci. Pollut. Res.* 23, 19350–19361.

- Ahmadi, M., Ghanbari, F., Alvarez, A., Martinez, S.S., 2017. UV-LEDs assisted peroxydisulfate/ Fe^{2+} for oxidative removal of carmoisine: the effect of chloride ion. *Korean J. Chem. Eng.* 34, 2154–2161.
- Ahmed, M.M., Barbati, S., Doumenq, P., Chiron, S., 2012. Sulfate radical anion oxidation of diclofenac and sulfamethoxazole for water decontamination. *Chem. Eng. J.* 197, 440–447.
- Amasha, M., Baalbaki, A., Ghauch, A., 2018. A comparative study of the common persulfate activation techniques for the complete degradation of an NSAID: the case of ketoprofen. *Chem. Eng. J.* 350, 395–410.
- Anipsitakis, G.P., Dionysiou, D.D., 2003. Degradation of organic contaminants in water with sulfate radicals generated by the conjunction of peroxydisulfate with cobalt. *Environ. Sci. Technol.* 37, 4790–4797.
- Antoniu, M.G., de la Cruz, A.A., Dionysiou, D.D., 2010. Degradation of microcystin-LR using sulfate radicals generated through photolysis, thermolysis and e(-) transfer mechanisms. *Appl. Catal. B* 96, 290–298.
- Asha, T.T., Gandhimathi, R., Ramaesh, S.T., Nidheesh, P.V., 2017. Treatment of stabilized leachate by ferrous-activated persulfate oxidative system. *J. Hazard. Toxic Radioact. Waste* 21, 04016012.
- Ayoub, G., Ghauch, A., 2014. Assessment of bimetallic and trimetallic iron-based systems for persulfate activation: application to sulfamethoxazole degradation. *Chem. Eng. J.* 256, 280–292.
- Babu, S.G., Aparna, P., Satishkumar, G., Ashokkumar, M., Neppolian, B., 2017. Ultrasound-assisted mineralization of organic contaminants using a recyclable LaFeO_3 and Fe^{3+} /persulfate Fenton-like system. *Ultrason. Sonochem.* 34, 924–930.
- Bautista, P., Mohedano, A.F., Casas, J.A., Zazo, J.A., Rodriguez, J.J., 2008. An overview of the application of Fenton oxidation to industrial wastewaters treatment. *J. Chem. Technol. Biotechnol.* 83, 1323–1338.
- Buxton, G.V., Greenstock, C.L., Helman, W.P., Ross, A.B., 1988. Critical review of rate constants for reactions of hydrated electrons, hydrogen atoms and hydroxyl radicals ($\bullet\text{OH}/\bullet\text{O}$) in aqueous solution. *J. Phys. Chem. Ref. Data* 17, 513–531.
- Chakma, S., Praneeth, S., Moholkar, V.S., 2017. Mechanistic investigations in sono-hybrid (ultrasound/ Fe^{2+} /UVC) techniques of persulfate activation for degradation of Azorubine. *Ultrason. Sonochem.* 38, 652–663.
- Chen, D., Ma, X.L., Zhou, J.Z., Chen, X., Qian, G.R., 2014. Sulfate radical-induced degradation of Acid Orange 7 by a new magnetic composite catalyzed peroxydisulfate oxidation process. *J. Hazard. Mater.* 279, 476–484.
- Chen, Y., Yang, S., Wang, K., Lou, L., 2005. Role of primary active species and TiO_2 surface characteristic in UV-illuminated photodegradation of Acid Orange 7. *J. Photochem. Photobiol., A* 172, 47–54.
- Cheng, X.W., Pan, G.P., Yu, X.J., 2015. Construction of high-efficient photoelectrocatalytic system by coupling with TiO_2 nano-tubes photoanode and active carbon/polytetrafluoroethylene cathode and its enhanced photoelectrocatalytic degradation of 2,4-dichlorophene and mechanism. *Chem. Eng. J.* 279, 264–272.
- Chu, W.H., Li, D.M., Deng, Y., Gao, N.Y., Zhu, Y.P., 2016. Effects of UV/PS and UV/ H_2O_2 pre-oxidations on the formation of trihalomethanes and haloacetonitriles during chlorination and chloramination of free amino acids and short oligopeptides. *Chem. Eng. J.* 301, 65–72.
- Criquet, J., Leitner, N.K.V., 2011. Electron beam irradiation of aqueous solution of persulfate ions. *Chem. Eng. J.* 169, 258–262.
- Deng, J., Shao, Y., Gao, N., Tan, C., Zhou, S., Hu, X., 2013. CoFe_2O_4 magnetic nanoparticles as a highly active heterogeneous catalyst of oxone for the degradation of diclofenac in water. *J. Hazard. Mater.* 262, 836–844.
- Deng, S., Xiao, X., Chen, G., Wang, L., Wang, Y., 2016. Cd doped porous Co_3O_4 nanosheets as electrode material for high perfor-

- mance supercapacitor application. *Electrochimica Acta* 196, 316–327.
- Deng, J., Ya, C., Ge, Y.J., Cheng, Y.Q., Cheng, Y.J., Xu, M.Y., 2018. Activation of peroxymonosulfate by metal (Fe, Mn, Cu and Ni) doping ordered mesoporous Co_3O_4 for the degradation of enrofloxacin. *RSC Adv.* 8, 2338–2349.
- Devi, L.G., Srinivas, M., ArunaKumari, M.L., 2016. Heterogeneous advanced photo-Fenton process using peroxymonosulfate and peroxydisulfate in presence of zero valent metallic iron: a comparative study with hydrogen peroxide photo-Fenton process. *J. Water Process Eng.* 13, 117–126.
- Du, Y.C., Ma, W.J., Liu, P.X., Zou, B.H., Ma, J., 2016. Magnetic CoFe_2O_4 nanoparticles supported on titanate nanotubes ($\text{CoFe}_2\text{O}_4/\text{TNTs}$) as a novel heterogeneous catalyst for peroxymonosulfate activation and degradation of organic pollutants. *J. Hazard. Mater.* 308, 58–66.
- Feng, Y., Lee, P.H., Wu, D., Shih, K., 2017. Rapid selective circumneutral degradation of phenolic pollutants using peroxymonosulfate-iodide metal-free oxidation: role of iodine atoms. *Environ. Sci. Technol.* 51, 2312–2320.
- Furman, O.S., Teel, A.L., Watts, R.J., 2010. Mechanism of base activation of persulfate. *Environ. Sci. Technol.* 44, 6423–6428.
- Gayathri, P., Dorathi, R.P.J., Palanivelu, K., 2010. Sonochemical degradation of textile dyes in aqueous solution using sulphate radicals activated by immobilized cobalt ions. *Ultrason. Sonochem.* 17, 566–571.
- Ghanbari, F., Martinez-Huitle, C.A., 2019. Electrochemical advanced oxidation processes coupled with peroxymonosulfate for the treatment of real washing machine effluent: a comparative study. *J. Electroanal. Chem.* 874, 113182.
- Ghanbari, F., Ahmadi, M., Cohari, F., 2019. Heterogeneous activation of peroxymonosulfate via nanocomposite $\text{CeO}_2\text{-Fe}_3\text{O}_4$ for organic pollutants removal: The effect of UV and US irradiation and application for real wastewater. *Sep. Purif. Technol.* 228, 115732.
- Ghauch, A., Tuqan, A.M., 2012. Oxidation of bisoprolol in heated PS/ H_2O systems: kinetics and products. *Chem. Eng. J.* 183, 162–171.
- Gordon, A.D., Smirnov, A., Shumlas, S.L., Singireddy, S., DeCesare, M., Schoonen, M.A.A., Strongin, D.R., 2013. Reduction of nitrite and nitrate on nano-dimensioned FeS. *Orig. Life Evol. Biospheres* 43, 305–322.
- He, Y., Jiang, D.B., Chen, J., Jiang, D.Y., Zhang, Y.X., 2018. Synthesis of MnO_2 nanosheets on montmorillonite for oxidative degradation and adsorption of methylene blue. *J. Colloid Interface Sci.* 510, 207–220.
- Hou, X.J., Shen, W.J., Huang, X.P., Ai, Z.H., Zhang, L.Z., 2016. Ascorbic acid enhanced activation of oxygen by ferrous iron: a case of aerobic degradation of rhodamine B. *J. Hazard. Mater.* 308, 67–74.
- Huang, K.C., Couttenye, R.A., Hoag, G.E., 2002. Kinetics of heat-assisted persulfate oxidation of methyl tert-butyl ether (MTBE). *Chemosphere* 49, 413–420.
- Huang, Y.F., Huang, Y.H., 2009. Behavioral evidence of the dominant radicals and intermediates involved in Bisphenol A degradation using an efficient $\text{Co}^{2+}/\text{PMS}$ oxidation process. *J. Hazard. Mater.* 167, 418–426.
- Jaafarzadeh, N., Ghanbari, F., Alvandi, M., 2017. Integration of coagulation and electro-activated HSO_5^- to treat pulp and paper wastewater. *Sustain. Environ. Res.* 27, 223–229.
- Ji, Y.F., Kong, D.Y., Lu, J.H., Jin, H., Kang, F.X., Yin, X.M., Zhou, Q.S., 2016. Cobalt catalyzed peroxymonosulfate oxidation of tetrabromobisphenol A: kinetics, reaction pathways, and formation of brominated by-products. *J. Hazard. Mater.* 313, 229–237.
- Khatiri, J., Nidheesh, P.V., Singh, S.A., Kumar, M.S., 2018. Advanced oxidation processes based on zero-valent aluminium for treating textile wastewater. *Chem. Eng. J.* 348, 67–73.
- Li, J.J., Liu, H.L., Cheng, X.W., Chen, Q.H., Ren, N.Q., 2013. Preparation and characterization of palladium/polypyrrole/foam nickel electrode for electrocatalytic hydrodechlorination. *Chem. Eng. J.* 225, 489–498.
- Li, X.L., Lu, H.J., Zhang, Y., He, F., 2017. Efficient removal of organic pollutants from aqueous media using newly synthesized polypyrrole/CNTs- CoFe_2O_4 magnetic nanocomposites. *Chem. Eng. J.* 316, 893–902.
- Li, R.H., Niu, J.M., Zhan, X.M., Liu, B., 2013. Simultaneous removal of nitrogen and phosphorus from wastewater by means of FeS-based autotrophic denitrification. *Water Sci. Technol.* 67, 2761–2767.
- Li, H., Wan, J., Ma, Y., Wang, Y., Guan, Z., 2015. Role of inorganic ions and dissolved natural organic matters on persulfate oxidation of acid orange 7 with zero-valent iron. *RSC Adv.* 5, 99935–99943.
- Li, N.W., Zheng, M.B., Chang, X.F., Ji, G.B., Lu, H.L., Xue, L.P., Pan, L.J., Cao, J.M., 2011. Preparation of magnetic CoFe_2O_4 -functionalized graphene sheets via a facile hydrothermal method and their adsorption properties. *J. Solid State Chem.* 184, 953–958.
- Liang, C., Bruell, C.J., Marley, M.C., Sperry, K.L., 2004. Persulfate oxidation for in situ remediation of TCE. I. Activated by ferrous ion with and without a persulfate-thiosulfate redox couple. *Chemosphere* 55, 1213–1223.
- Lin, Y.T., Liang, C., Chen, J.H., 2011. Feasibility study of ultraviolet activated persulfate oxidation of phenol. *Chemosphere* 82, 1168–1172.
- Lin, C.C., Wu, M.S., 2014. UV/ $\text{S}_2\text{O}_8^{2-}$ process for degrading polyvinyl alcohol in aqueous solutions. *Chem. Eng. Process. Process Intensif.* 85, 209–215.
- Liu, L., Zhu, Y.-P., Su, M., Yuan, Z.Y., 2015. Metal-free carbonaceous materials as promising heterogeneous catalysts. *Chem-CatChem* 7, 2765–2787.
- Lutze, H.V., Bircher, S., Rapp, I., Kerlin, N., Bakkour, R., Geisler, M., von Sonntag, C., Schmidt, T.C., 2015. Degradation of chlorotriazine pesticides by sulfate radicals and the influence of organic matter. *Environ. Sci. Technol.* 49, 1673–1680.
- Nafey, A.A., Addad, A., Sieber, B., Chastanet, G., Barras, A., Szunerites, S., Boukherroub, R., 2017. Reduced graphene oxide decorated with Co_3O_4 nanoparticles (rGO- Co_3O_4) nanocomposite: a reusable catalyst for highly efficient reduction of 4-nitrophenol, and Cr(VI) and dye removal from aqueous solutions. *Chem. Eng. J.* 322, 375–384.
- Neppolian, B., Doronila, A., Ashokkumar, M., 2010. Sonochemical oxidation of arsenic (III) to arsenic (V) using potassium peroxydisulfate as an oxidizing agent. *Water Res.* 44, 3687–3695.
- Neta, P., Madhavan, V., Zemel, H., Fessenden, R.W., 1977. Rate constants and mechanism of reaction of $\text{SO}_4\cdot^-$ with aromatic compounds. *J. Am. Chem. Soc.* 99, 163–164.
- Nidheesh, P.V., Rajan, R., 2016. Removal of rhodamine B from a water medium using hydroxyl and sulphate radicals generated by iron loaded activated carbon. *RSC Adv.* 6, 5330–5340.
- Popat, A., Nidheesh, P.V., Singh, T.S.A., Kumar, M.S., 2019. Mixed industrial wastewater treatment by combined electrochemical advanced oxidation and biological processes. *Chemosphere* 237, 124419.
- Rastogi, A., Ai-Abed, S.R., Dionysiou, D.D., 2009. Sulfate radical-based ferrous-peroxymonosulfate oxidative system for PCBs degradation in aqueous and sediment systems. *Appl. Catal. B* 85, 171–179.
- Ren, Y., Lin, L., Ma, J., Yang, J., Feng, J., Fan, Z., 2015. Sulfate radicals induced from peroxymonosulfate by magnetic ferrosin MF Fe_2O_4 (M = Co, Cu, Mn, and Zn) as heterogeneous catalysts in the water. *Appl. Catal. B* 165, 572–578.
- Rida, T., Othmane, A., Younes, E., 2018. Magnetic CoFe_2O_4 nanoparticles supported on graphene oxide ($\text{CoFe}_2\text{O}_4/\text{GO}$) with high catalytic activity for peroxymonosulfate activation and degradation of rhodamine B. *RSC Adv.* 8, 1351–1360.
- Rivas, J., Solis, R.R., Gimeno, O., Sagasti, J., 2015. Photocatalytic elimination of aqueous 2-methyl-4-chlorophenoxyacetic acid in the

- presence of commercial and nitrogen-doped TiO₂. *Int. J. Environ. Sci. Technol.* 12, 513–526.
- Salunkhe, R.R., Tang, J., Kamachi, Y., Nakato, T., Kim, J.H., Yamauchi, Y., 2015. Asymmetric supercapacitors using 3D nanoporous carbon and cobalt oxide electrodes synthesized from a single metal-organic framework. *ACS Nano* 6, 6288–6296.
- Sarath, K., Gandhimathi, R., Ramesh, S.T., Nidheesh, P.V., 2014. Removal of reactive magenta-MB from aqueous solution by persulphate-based advanced oxidation process. *Desalin. Water Treat.* 57, 11872–11878.
- Senthilnathan, N., Nachiappana, P.G., 2015. Treatment of pharmaceutical effluent using novel heterogeneous fly ash activated persulfate system. *J. Environ. Chem. Eng.* 3, 2229–2235.
- Sharma, J., Mishra, I.M., Dionysiou, D.D., Kumar, V., 2015. Oxidative removal of Bisphenol A by UV-C/peroxymonosulfate (PMS): Kinetics, influence of co-existing chemicals and degradation pathway. *Chem. Eng. J.* 276, 193–204.
- Sharma, J., Mishra, I.M., Kumar, V., 2016. Mechanistic study of photo-oxidation of Bisphenol-A (BPA) with hydrogen peroxide (H₂O₂) and sodium persulfate (SPS). *J. Environ. Manage.* 166, 12–22.
- Sun, H.M., Yang, X.J., Zhao, L.J., Xu, T.H., Lian, J.S., 2016. One-pot hydrothermal synthesis of octahedral CoFe/CoFe₂O₄ submicron composite as heterogeneous catalysts with enhanced peroxymonosulfate activity. *J. Mater. Chem. A* 4, 9455–9465.
- Wang, Y.X., Sun, H.Q., Ang, H.M., Tade, M.O., Wang, S.B., 2015. 3D-hierarchically structured MnO₂ for catalytic oxidation of phenol solution by activation of peroxymonosulfate: structure dependence and mechanism. *Appl. Catal. B* 164, 159–167.
- Wang, X.K., Wang, J.G., Guo, P.Q., Guo, W.L., Wang, C., 2009. Degradation of rhodamine B in aqueous solution by using swirling jet-induced cavitation combined with H₂O₂. *J. Hazard. Mater.* 169, 486–491.
- Wang, Q., Wang, B.B., Ma, Y., Xing, S.T., 2018. Enhanced superoxide radical production for ofloxacin removal via persulfate activation with Cu-Fe oxide. *Chem. Eng. J.* 354, 473–480.
- Wang, Z., Yuan, R., Guo, Y., Xu, L., Liu, J., 2011. Effects of chloride ions on bleaching of azo dyes by Co²⁺/oxone reagent: kinetic analysis. *J. Hazard. Mater.* 190, 1083–1087.
- Xie, W., Dong, W., Kong, D., Ji, Y., Lu, J., Yin, X., 2016. Formation of halogenated disinfection by-products in cobalt-catalyzed peroxymonosulfate oxidation processes in the presence of halides. *Chemosphere* 154, 613–619.
- Yang, Q., Choi, H., Al-Abed, S.R., Dionysiou, D.D., 2009. Iron-cobalt mixed oxide nanocatalysts: heterogeneous peroxymonosulfate activation, cobalt leaching, and ferromagnetic properties for environmental applications. *Appl. Catal. B* 88, 462–469.
- Zacharias, F., Eduard, M.M., Joannis, K., 2016. Removal of cibacron black commercial dye with heat- or iron-activated persulfate: statistical evaluation of key operating parameters on decolorization and degradation by-products. *Desalination Water Treat.* 57, 2616–2625.
- Zhang, J., Chen, M.Y., Zhu, L., 2016. Activation of persulfate by Co₃O₄ nanoparticles for orange G degradation. *RSC Adv.* 6, 758–768.
- Zhang, T., Zhu, H., Croue, J.P., 2013. Production of sulfate radical from peroxymonosulfate induced by a magnetically separable CuFe₂O₄ spinel in water: efficiency, stability, and mechanism. *Environ. Sci. Technol.* 47, 2784–2791.
- Zuo, Z.H., Cai, Z.L., Katsumura, Y., Chitose, N., Muroya, Y., 1999. Reinvestigation of the acid-base equilibrium of the (bi)carbonate radical and pH dependence of its reactivity with inorganic reactants. *Radiat. Phys. Chem.* 55, 15–23.